

Optical Engineering

OpticalEngineering.SPIEDigitalLibrary.org

Traceable technique for an *in situ* full field in-plane measurement validation of digital image correlation

Eszter Szigeti
Matthew Loparco
Evgeni Todorov
Shelby Wheatley
Richard J. Greene

SPIE.

Eszter Szigeti, Matthew Loparco, Evgeni Todorov, Shelby Wheatley, Richard J. Greene, "Traceable technique for an *in situ* full field in-plane measurement validation of digital image correlation," *Opt. Eng.* **56**(3), 033101 (2017), doi: 10.1117/1.OE.56.3.033101.

Traceable technique for an *in situ* full field in-plane measurement validation of digital image correlation

Eszter Szigeti,^{a,*} Matthew Loparco,^a Evgeni Todorov,^a Shelby Wheatley,^a and Richard J. Greene^b

^aAirbus Operations Ltd., UK, Filton, Bristol, United Kingdom

^bStrain Solutions Ltd., Dunston Innovation Centre, Chesterfield, Derbyshire, United Kingdom

Abstract. For digital image correlation to be firmly accepted as a validated displacement measurement system in the industrial arena, a measurement must be captured by the analysis system at time of test which confirms that the image correlation hardware and software system is performing as expected. To this end, a method for validating stereo digital image correlation optical test setups is presented, which is traceable to the length standard. The method employs a screen, on which is displayed a randomized speckle pattern of appropriate pitch for the test in question. This speckle pattern is then artificially translated by a known number of pixels on the screen, and image pairs captured of the original and translated speckles. Processing of these data image pairs with image correlation, and calibration of the pixel pitch of the display screen using a traceable measurement system, allows the image correlation test setup to be traceably calibrated in terms of in-plane displacement. The method is shown to be sufficiently sensitive and repeatable to provide a reasonably accurate, traceable validation in a practical environment. © The Authors. Published by SPIE under a Creative Commons Attribution 3.0 Unported License. Distribution or reproduction of this work in whole or in part requires full attribution of the original publication, including its DOI. [DOI: [10.1117/1.OE.56.3.033101](https://doi.org/10.1117/1.OE.56.3.033101)]

Keywords: digital image correlation; validation.

Paper 161575 received Oct. 10, 2016; accepted for publication Feb. 9, 2017; published online Mar. 2, 2017.

1 Introduction

Digital image correlation (DIC) is a powerful optical measurement technique that provides full-field displacement and strain data for a test specimen undergoing deformation. Postprocessing software then tracks $N \times N$ pixel subset areas within the image pairs using a random speckle pattern applied to the surface of the specimen. DIC has been shown to be a powerful technique in both the validation¹ and revision² of numerical models, such as finite element simulations, as it can provide a full-field data map contrary to traditional methods of comparing a model to point measurements provided by strain gauges. Methodologies have been further developed for the comparison between numerical data from simulation and experimental data from optical measurements. However, in order for DIC to be accepted as a traceable measurement, it must be shown to be a calibrated measurement technique, traceable to a recognized measurement standard by a continuous chain of comparisons.

The most current measurement calibration methods for DIC propose the use of a standardized reference specimen to provide a “known” theoretically predicted displacement or strain field. This data can then be compared to the experimental optical measurements in order to quantify an uncertainty value for those measurements. First, the SPOTS project developed³ and provided guidelines⁴ for the use of two reference specimens: a Brazilian disc;⁵ and a monolithic four point bend beam for the evaluation and calibration of optical measurements.⁶ Designed for use in terms of strain measurement, the calibration specimens achieve traceability

to the standard for length through the use of a displacement transducer.

The VANESSA project, a continuation of the SPOTS project, developed a calibration method with the focus on using optical techniques to validate computational solid mechanics models.⁷ The outcomes of these projects propose the use of a cantilever beam reference material for static or dynamic loading cases in order to provide a “known” displacement/strain field and a calibrated displacement transducer to provide traceability to the standard of length for out-of-plane static loading.

This article proposes a measurement calibration procedure that uses a commercially available, high quality screen, such as a tablet or a high-definition television, to display artificially generated images of known deformation/displacement fields. The images are captured by a DIC stereo camera pair, having previously undergone a system calibration in terms of the intrinsic properties (lens distortion, focal length, sensor alignment, etc.) and extrinsic properties (distance and angles between cameras) of the setup, and are then postprocessed to produce measurements of the displayed deformation. With the known characteristics of the screen and the images, deviations between the imposed deformation displayed and the measured deformation will represent the uncertainty of measurements performed by that particular setup. While using digital screens as reference for DIC measurements has been done before, it has not been used for top-down quantification of the measurement error.⁸ The method is fully described in European Patent Application EP 30 26 632 AP.⁹

The core idea of the method is to make DIC measurements more acceptable in an industrial setting. In industry, stereo cameras are often used for measurements of flat or initially flat specimens, undergoing in-plane deformation, since a stereo optical setup deals better with misalignment,

*Address all correspondence to: Eszter Szigeti, E-mail: eszter.szigeti@airbus.com

interference, and other practical challenges. Nevertheless, the typically observed deformations are predominantly in-plane and can be emulated by pixel-shift translations on a digital screen. Using inexpensive, off-the-shelf equipment provides an attractive method to achieve a traceable, if potentially less accurate, validation of the measurement. The method follows the top-down approach of error quantification, measuring the resulting error instead of quantifying each individual source of uncertainty.

The proposed method provides a solution for ensuring DIC is a traceable measurement technique directly via the display screen itself. This is achieved through the precise measurement of the screen's pixel pitch using a calibrated device, such as a microscope, creating a traceable measurement chain back to the length standard. It is intended that the measurement calibration can be further developed and expanded to any size screen in order to represent multiple test setups, and has the capability to display images representing various types and magnitudes of deformation. In addition, high-resolution screens with a high pixel density could be custom made for the purpose, improving and extending the applicability of the method.

This article evaluates the proposed measurement calibration method using a third-generation, 9.7-in. Apple iPad Air with a screen resolution of 2048×1536 pixels (264 ppi)¹⁰ and a second-generation, 6-in. Kindle Paperwhite with a screen resolution of 1200×825 pixels (212 ppi)¹¹ as display screens to show images representing rigid body in-plane translations. This article will first describe the experimental method behind the technique, including its route for traceability and the setup used in testing. It will then present results from these tests and subsequent discussions and conclusions, including proposals for further research.

2 Experimental Method

2.1 Traceability

Within this technique, traceability is achieved to the standard of length through the measurement of the pixel pitch of the display screen, as shown in Fig. 1.

For the purpose of this investigation, the technique was applied to both liquid crystal display (LCD) and electronic paper display (EPD) screens. A ZEISS Axio Imager. M1m microscope with AxioCam HRC was used to verify the screen manufacturer pixel pitch specification and provide traceability.

The microscope was calibrated for measurement in ZEISS AxioVision Rel 4.8 software using a $100 \times 0.1 = 10$ mm Pyser-SGI Ltd. PS1R stage micrometer graticule, which in turn was within the validity of its calibration, completed in accordance to UKAS requirements to give an expanded measurement uncertainty of $\pm 0.5 \mu\text{m}$ at $20.0 \pm 1^\circ\text{C}$. This was achieved by performing three repeated measurements using a laser interferometer of each 1 mm graduation on the scale of the graticule from 1 to 10 mm. A single

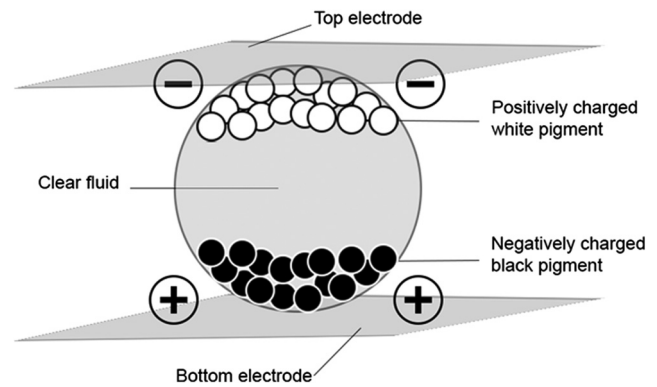


Fig. 2 Schematic view of one capsule from within the ink capsule layer of an E-ink screen.

value for combined standard uncertainty was calculated using the root sum square of the standard deviations of each set of repeated measurements. The expanded measurement uncertainty value of $\pm 0.5 \mu\text{m}$ at $20.0 \pm 1^\circ\text{C}$ was then calculated using a coverage factor, $k = 2$ to provide a confidence level of 95%.

The laboratory in which the pixel pitch measurements were performed was temperature controlled at 21°C . It was verified that the effect of thermal expansion of the glass plate of the graticule was insignificant in relation to the expanded measurement uncertainty by calculating that a temperature change of $\pm 1^\circ\text{C}$ would induce a length change in the glass of ± 90 nm over the length of the graticule (using a coefficient of thermal expansion for glass of 9×10^{-6} per $^\circ\text{C}$ at 20°C).¹²

Measurements of pixel clusters were taken at 12 regularly spaced intervals around the LCD and EPD screens (each cluster defined as one group of red, green, and blue subpixels for the LCD screen and one black pixel for the e-ink screen). The LCD screen was removed from the casing and deconstructed until the color filter layer was revealed. Measurements were completed on this layer because it is assumed to most accurately represent the fixed dimension of each subpixel used to display an image.

The EPD screen was not deconstructed because it does not have the same layer construction as LCD screens. Therefore, pixel pitch measurements were carried out on the fully assembled screen, concentrating on the ink capsule layer, Fig. 2.

The repeatability of the operator's measurements was assessed by measuring each set of pixels using $10\times$, $20\times$, and $50\times$ objective lenses, respectively. This range of lenses was selected because it represents both the smallest and largest magnifications where defined pixel edges are visible and the distance between at least two pixel clusters can be measured. For each image, a horizontal (X -axis) and vertical (Y -axis) sequence of pixels was counted and measured using the AxioVision Release 4.7 software package. Each

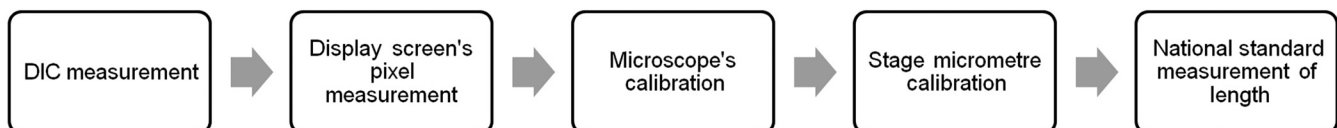


Fig. 1 Traceability chain for calibration method.

Table 1 Final pixel pitch values.

Direction	LCD pixel pitch (μm)	EPD pixel pitch (μm)
X	95.99	120.67
Y	96.02	120.21

measurement was then divided by the number of pixels counted to give the average pixel pitch for each magnification. Final pixel pitch values were then obtained by averaging the pixel pitch in the *X* and *Y* directions across all magnifications, Table 1.

An example image of pixels as viewed under the microscope is shown in Fig. 3.

2.2 Pixel Pitch Measurement Uncertainty

The overall accuracy of the pixel pitch measurements is a combination of both the calibrated hardware/software and operator accuracy.

The hardware and software accuracy is $0.635 \mu\text{m}$. The value is taken directly from the calibration certificate. This is a summation of the calibration's variation of measurement and uncertainty of measurement, averaged over both grati-cules used.

Operator accuracy was determined from the difference in measurements of the same pixels at different magnification. The uncertainty in this process stems from the variability in manually selecting the same point on each pixel in the image due to the lack of clearly defined edges of the screen pixels. Operator accuracy was determined by averaging the maximum variation in pixel pitch of the same pixel cluster for each magnification case. This assumes that the same pixel cluster is being measured for each of the magnifications. The average was then taken and multiplied by the microscope's camera image pixel dimension at each given magnification and divided by the average number of pixel clusters measured at each magnification to give an overall user accuracy presented in Table 2.

The combined overall uncertainty is quantified in Table 3.

Table 2 Microscope measurement uncertainty—user.

Magnification	Microscope camera pixel dimension (μm) ^a	Average number of tablet pixels measured	Operator accuracy (μm)
10×	2.060	9	0.2889
20×	1.008	4	0.1495
50×	0.5038	2	0.1751

^aAccording to microscope calibration.

Table 3 Microscope measurement uncertainty—overall.

Magnification	Overall uncertainty (μm)
10×	0.9239
20×	0.7845
50×	0.8101

2.3 Test Set-Up

Tests were performed in a temperature-controlled laboratory at 21°C . DIC data capture used a pair of Allied Vision Technologies Dolphin F201-B 2 megapixel, $1/1.8''$ sensor cameras with 12-mm focal length Schneider C-mount lenses at an $f/11$ aperture. This combination of lens and sensor demonstrates reasonable optical distortions (see κ -values in Table 4) and the aperture was chosen to provide a large depth of field for the experiment, while minimizing the effects of diffraction. For each test, the DIC system was set up in a conventional manner, with stand-off distance approximately twice the camera separation distance to give a camera angle of $\sim 30^\circ$, which was accurately confirmed to 28.645° as parameter β from Table 4. The field of view was optimized to match the screen dimensions as closely as possible to utilize as many camera image pixels as possible.

A system calibration was performed, using Correlated Solutions' image acquisition software Vic-Snap 8 and post-processing software Vic-3D 7, for application to all data

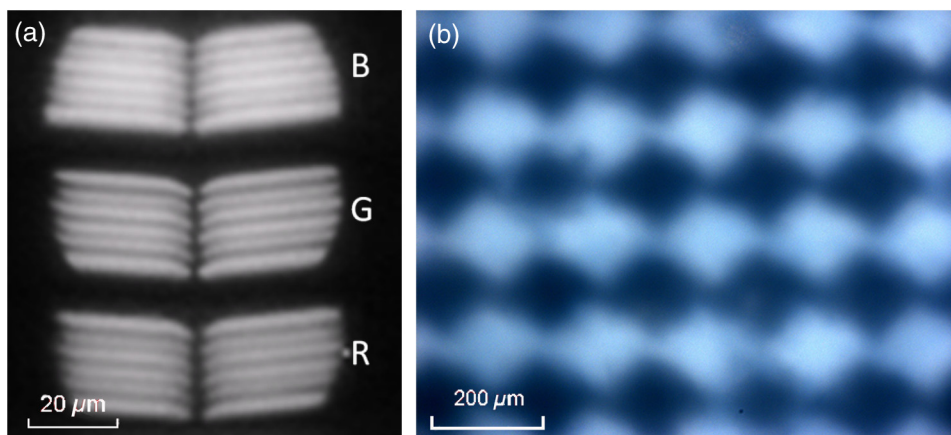
**Fig. 3** Close-up of the pixels of the different display types.

Table 4 Typical two- and three-dimensional camera calibration parameters for a calibration score of 0.021 px presented for repeatability. Camera model and parameter naming follows standard convention.¹³

Individual cameras			Camera system	
Parameter (unit)	Camera 1	Camera 2	Parameter (unit)	Value
Center (<i>X</i>) (px)	825.5 ± 1.1	817.3 ± 0.8	α (deg)	0.088
Center (<i>Y</i>) (px)	627.2 ± 0.5	641.6 ± 0.5	β (deg)	28.645
Focal length (<i>X</i>) (px)	2871.5 ± 1.1	2864.3 ± 1.1	γ (deg)	0.120
Focal length (<i>Y</i>) (px)	2871.5 ± 1.3	2864.6 ± 1.3	T_x (mm)	-149.780
Skew (-)	-0.317 ± 0.01	0.123 ± 0.01	T_y (mm)	0.032
Distortion κ_1	-0.151 ± 0.0	-0.138 ± 0.0	T_z (mm)	37.845 ± 0.003
Distortion κ_2	0.234 ± 0.0	0.165 ± 0.0		

analysis. The system calibration builds a model of the physical system in the software using intrinsic characteristics such as the focal length and distortion of the cameras, extrinsic characteristics such as the distance and angles between the cameras, and the geometry of a calibration board that consists of a number of control points with a fixed pitch. For these tests, a calibration board with 9.02 mm spacing between control points was used. Thirty image pairs of the calibration board at different angles and orientations were taken within a 200-mm deep control volume of the stand-off distance with the cameras at an exposure time of 41.5 ms. These images were then imported into the DIC postprocessing software and analyzed with respect to the 9.02 mm target used. This method achieved a calibration score of <0.022 px for both LCD and EPD screen experiments. This score corresponds to the average distance in camera image pixels between a theoretical point predicted by the model and its actual position in the image. A detailed overview of typical camera system calibration parameters is given in Table 4.

An ideal reference speckle image was sourced from an image database supplied by the Metrology Workgroup of the French CNRS research network 2519 “Mesures de Champs et Identification en Mecanique des Solides/ Full-Field Measurements and Identification in Solid Mechanics.”¹⁴ The scale and resolution of this image were then cropped using Photoshop CS5 to provide an “optimal” 3-5 camera image pixels per speckle for the resolution of each display screen. After this, the resolution of the speckle image was fixed to match that of the display screen. This speckle pitch has been shown to give optimal results in terms of spatial resolution and measurement accuracy.¹⁵ The displacement images were then created by applying integer number of screen pixel shifts to this image in the *X* and *Y* directions.

Prior to photographing the digitally translated speckle patterns with the stereo DIC system, the success of the numerical screen pixel translations between images was verified by subtracting the relevant columns/rows of the translated images from the reference speckle image. The images were converted into 0–255 gray level matrices and subtracted from each other to verify that the subtraction

result was a null field all zero entries which was the case for all translations.

Three shift cases were generated for the *X*- and *Y*-axes, each with 1, 5, and 10 screen pixel step sizes, as shown in Table 5.

These cases were chosen to be representative of the various test envelopes performed during structural testing of aerospace components, portraying maximum displacements of ~2 mm, 10 mm, and 20 mm, for each case, respectively.

For each shift case, a sequence of 21 images was generated. Each starts with the reference image which is then shifted by the step size 20 times to the maximum shift value. Sample shifted speckle images of 0 px, 5 px, and 10 px image shifts can be seen in Fig. 4.

Tests were also conducted to investigate the effect, if any, of image persistence or retention, an occurrence on LCD and EPD screens wherein a remnant of the previous image may be present in the following image. All shift cases were recaptured with a fully saturated white image presented in between each shift image to erase any trace of the previously presented image. This was found to have a statistically insignificant effect on the LCD screen results but significant effect on the EPD screen. Therefore, all shift cases on EPD screens were captured using a fully saturated white image between each shift image.

Furthermore, an investigation into the use of the backlight built into LCD and EPD screens during the experiment was also conducted. All cases of shifts were recaptured with full screen backlight brightness and minimum possible backlight brightness for each screen. These cases were then postprocessed and the overall error of the measurements compared. From the data, the use of backlight was found to have an

Table 5 Shift cases in screen pixels.

Case	Step (px)	Maximum shift (px)
Case 1	1	20
Case 5	5	100
Case 10	10	200

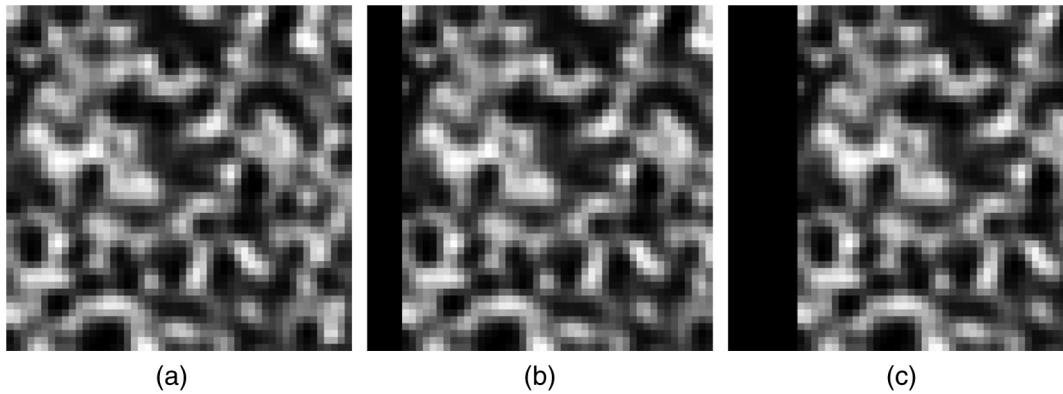


Fig. 4 Sample shifted speckle images.

insignificant effect on the LCD screen results but significant effects on EPD screen results with up to 0.07 screen pixels greater maximum measurement error observed in results using no backlight versus results using full backlight brightness.

During all tests, the screen was supported so that it remained physically stationary and perpendicular to the DIC system throughout the data capturing process. For each of the three X and three Y shift cases, the shift images were displayed in order from the zero pixel shift reference image to the maximum shift, a total of 21 images. The shift images were presented using a slideshow format to ensure there was no movement of the screen by the operator between shifts. DIC data capture software was used to capture each shift image three times giving a total of 63 images and each shift case was captured three times over three days to ensure repeatability. The time each screen was on before capture was found not to influence the measurements, which is expected since temperature of the screens remain close to ambient. A temperature fluctuation of $<1^\circ\text{C}$ was measured for the EPD during extended operation, both with and without backlight. Temperature change effects are thus considered negligible. It was also ensured that ambient lighting did not change significantly during the capture process.

2.4 Postprocessing

The images were initially postprocessed using an area of interest and coordinate system (set using three point selection) chosen as shown in Fig. 5. The origin and x - and y -axis points of the coordinate system translation were selected at the same pixel cluster in each analysis. It was calculated that a small misalignment between the coordinate system assigned in the postprocessing software and that of the display screen/shift images had a negligible effect on the resultant data. This can be illustrated as follows: assume that during selection, the second point establishing the x -axis deviates by 10 camera image pixels from the actual x -axis of the screen. This is a very conservative estimation, since a typical deviation in selecting points on a sharp image is 1 to 2 pixels. For the EPD screen, the shorter of the two targets, with ~ 1000 camera image pixels between the two picking points, this results in a misalignment angle $\alpha = \tan^{-1} \frac{10 \text{ px}}{1000 \text{ px}} \approx 0.01$. From straightforward trigonometry, the difference in the measured and actual displacement would be $1 - \cos \alpha \approx 0.005\%$. This error is very much

negligible when compared with the $\approx 0.1\%$ to 1% uncertainty of pixel pitch measurement.

This was additionally investigated by repeating the analysis of a set of shift images and changing the particular pixel chosen for the origin, x - and y -axis points by a few camera image pixels in each direction in each analysis. Furthermore, the default best plane fit coordinate system was also evaluated using the same comparison method. By comparing the produced error and standard deviation results in both investigations, it could be observed that the small changes in the selected coordinate system had an insignificant consequence on the values. As a result, all subsequent measurements were postprocessed using the default best plane fit coordinate system.

The subset size, which determines the size of the data facet that is tracked across time, was set at 25×25 camera image pixels so as to be sufficiently large to contain a distinct speckle pattern while still computing results in a reasonable time. Equally, the step size, which determines how many data facets are tracked, was set at five camera image pixels as a compromise between providing an acceptable amount of data points and calculation time, yielding $\sim 55,000$ data points on each image of each translation case. In addition, a seed point was added in the analysis area, at approximately the same point on the speckle for each analysis, in order to ensure the correlation ran smoothly with the larger pixel shifts. Although not required for successful correlation,

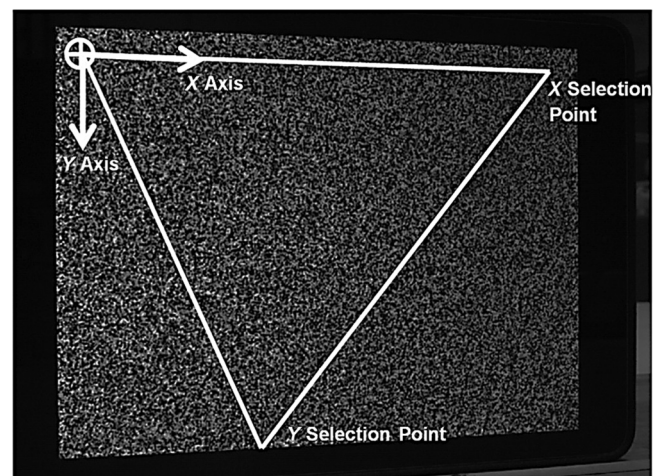


Fig. 5 Vic 3-D area of interest—LCD screen.

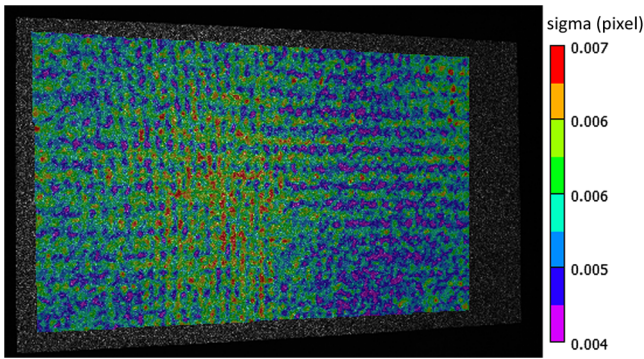


Fig. 6 Sample sigma—LCD screen.

the seed point was also added to the analysis of the smaller shifts in order to keep consistency between tests.

Data were exported in the form of a mean and standard deviation of displacement in only X or Y depending on which parameter was shifted for each image. These are mean and standard deviation values over the whole area of interest of each correlation. Exported data were then averaged across all repeated tests to achieve a single value for each X and Y shift. These values were then converted from meters (from camera calibration) to screen pixels by dividing them by the appropriate X or Y pixel pitch value from Table 1. This method was also used to achieve a single standard deviation value, in screen pixels, for each shift. Error, normalized error, and standard deviation of measurement for each shift case were then graphically displayed to assess the overall error of the system.

Error and normalized error were calculated according to Eqs. (1) and (2), respectively. Normalization has the benefit of presenting the results in a manner that clearly portrays the relationship between the magnitude of the error and the magnitude of the measurement.

$$\text{Error} = \text{imposed shift} - \text{measured shift}, \quad (1)$$

$$\text{Normalized error} = \left| \frac{\text{error}}{\# \text{ of pixels shifted}} \right|. \quad (2)$$

Further to the calculated measurement errors, the DIC post-processing software also calculates a confidence margin of the results, known as the sigma value, which indicates how well each subset of data is tracked between shifts. A sigma value of zero indicates a perfect match while higher numbers can indicate a poor match. Figure 6 shows the DIC post-processing software calculated sigma values for a 200-pixel X -axis shift. Across all the measurements taken, all data are reported with an average sigma range of 0.004 to 0.007 camera image pixels.

3 Results

3.1 Difference Between Screen Axes

Figure 7 shows the error for large displacements of the DIC measurement at each imposed pixel shift for the two different screens. Pixel shifts are imposed along the long (X) and short (Y) axes of the screen (see also Fig. 5). The error is calculated according to Eq. (1) and as discussed in Sec. 2.4. Several important observations can be made based on the figure.

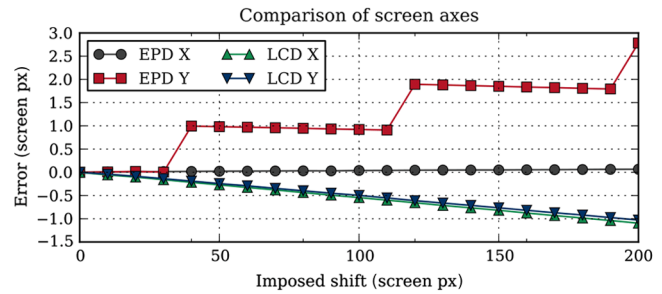


Fig. 7 The error in pixels is linear with the imposed pixel shift, which suggests constant normalized error in pixels. The two axes of the LCD screen behave similarly. The short axis on the E-Ink (EPD) screen shows a 1-px step in the error at 40, 120, and 200 px.

First, a linear relationship between the imposed shift and the error is evident for both the EPD and LCD screens. This is consistent with a constant normalized error (error per pixel) as discussed further in Sec. 3.3.

The error along X and Y for the LCD screen is approximately equal. This suggests little difference either between the properties of the screen along the axes or the performance of the DIC setup and algorithm. However, the error along the y -axis of the EPD screen is much larger than along the x -axis, due to steps one screen pixel at pixel shifts of 40, 120, and 200. On further inspection, including repeating the test with a rotated screen to ensure no optical effect outside of the screen is responsible, it is concluded that this error is a result of the screen construction, which is slightly different between the X and Y directions.

The well-defined behavior of the bias (1 px for every 80 px, starting at 40) suggests that a more involved methodology (e.g., not shifting the image from the edge, correcting for the known bias, etc.) for displacing the image on the screen might resolve the issue. However, in its current form, the method still allows for unbiased validation of displacements up to 40 screen pixels, or ~ 4 mm.

Since the LCD screen behaves similarly in both principal directions, all further results displayed are for displacement along the long (X) axis of the screen unless explicitly specified.

3.2 Standard Deviation

A clear sinusoidal dependence of the standard deviation of measurement on the imposed shift can be observed in Fig. 8 for all three different steps. A similar sinusoidal pattern of one camera image pixel period is observed in standard deviation of error in DIC due to the periodicity of the properties of the camera sensors used in the image discretization process.¹⁶ (While standard deviation of error and standard deviation of measurement are distinct statistical properties, they behave similarly if the sample size is sufficiently large.) However, the sinusoidal patterns observed on the figure have different periods for the different step sizes. This is explained with the very close size of camera pixel and imposed displacements. The aliasing effect observed is similar to sampling a wave at sampling frequency lower than the Nyquist frequency of the wave. Depending on the sampling frequency, the wave appears to have different (lower) frequencies. On Fig. 8, the step size is equivalent to the sampling rate.

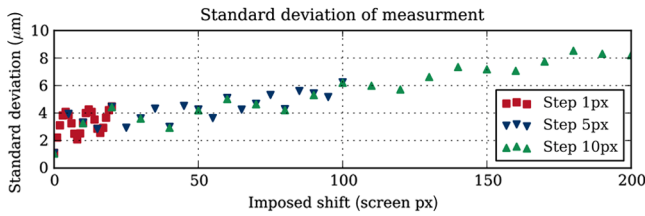


Fig. 8 The standard deviation of the measurement shows a sinusoidal dependency, with a frequency dependent on the sampling step. The sinusoidal behavior dominates at small displacement, while an additional linear dependence is apparent at larger shifts.

A linear dependence appears to be added to the sinusoidal behavior. Its distribution among different sources might represent interest for further investigation, but is beyond the scope of the current discussion. Nevertheless, the fact that standard deviation of measurement exhibits discretization error behavior shows that measurements taken from a screen do not introduce large unexpected random error which is hidden in the rest of the results by the averaging process.

3.3 Difference Between Screens

Figure 9 shows the main results of the evaluation of the method. The normalized error is calculated as detailed in Eq. (2). Two different length scales are shown to illustrate the short-range and long-range behaviors of the error.

The plot on the right-hand side of Fig. 9 shows the behavior of the normalized error (error per pixel, in percent) at large displacement scales. The constant nature of the phenomenon is expected, since it is consistent with error in the pixel pitch measurement, which has relatively large uncertainty.

The size of the normalized error, on average about 0.5% for the LCD and 0.05% for the EPD, is well within the minimum necessary to perform a useful validation, which suggests that both screens can be used in practice. However, since similar a setup was used to evaluate both types of screens, it can be reasoned that the EPD will add much smaller traceable uncertainty to the measurement, despite the larger screen pixel size.

The small-scale displacement plot on the left-hand side of Fig. 9 shows the normalized error at small scales, up to a pixel shift equivalent to ~2 mm of displacement. The EPD normalized error starts higher than the LCD error.

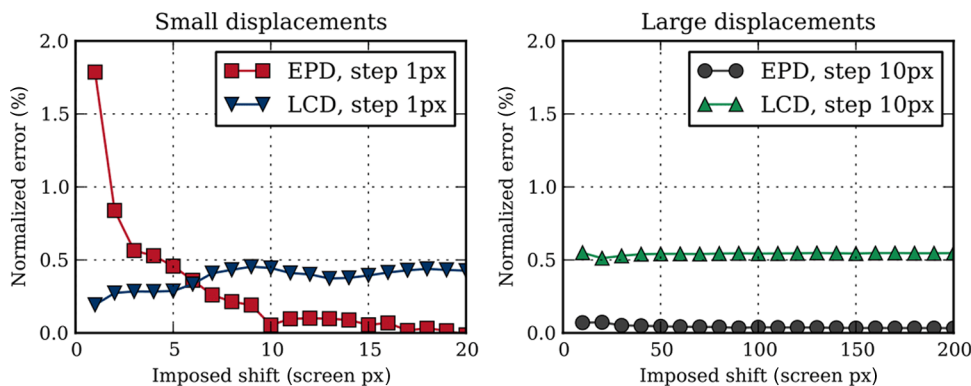


Fig. 9 For large displacements, the normalized error is approximately constant, with E-Ink (EPD) screen having an order of magnitude smaller error than the LCD. At very small displacements, LCD screens provide smaller error, but EPD error decreases very quickly with increasing displacement.

The reasons behind this can be numerous, but should in general be attributed to the type of screen, as the LCD uses a similar setup but has much smaller normalized error. Nevertheless, the error of the EPD falls quickly with the imposed shift and becomes comparable with LCD for displacements larger than 500 μm .

Figure 9 shows that all sources contributing to the error of the DIC measurement in the current study add up to ~0.1% to 1%, depending on the configuration. Since part of the error is setup dependent, the error introduced by using a screen with relatively large pixel pitch uncertainty is at most within the same range.

4 Discussion

A number of prior developments to validate DIC output focus on strain measurements. In its current form, the method has not been tested in validating strain or out-of-plane measurements. However, even without further development and using established technology, Fig. 9 shows that the method can be used to provide displacement validation to an accuracy of 0.1% to 1%, which is sufficient for many structural testing applications.

The top-down approach has limitations in determining the contribution of each individual source, since many apparent and hidden sources of error are present. However, as discussed in Sec. 3.2, the influences of some sources can be dominant in specific arrangements.

The main advantages of the proposed method lie in the flexibility and simplicity of application. Methods relying on physical artifacts often require means of deforming the artifact, which can present practical challenges in an industrial environment. The proposed method requires a single device. The screen can display multiple speckle patterns and cover a large range of deformations, with the minimum achievable simulated displacement limited by the physical size of a single display pixel. In practical situations, the screen can easily be moved to different positions and orientations, to provide validation for different areas of specimens of complex geometry. The main constraint on the flexibility is that in its current form the method allows validation of the displacement only in the plane of the screen.

The measurement calibration method described within this article was also replicated on AG Neovo RX-W32¹⁷ and LG 4K LCD¹⁸ television screens using a similar setup. A sample set of speckle images were presented on

the screen, captured and postprocessed using the same method as reported in this article. The obtained results for error, normalized error, and standard deviation were found to be statistically comparable to those reported above providing evidence that the proposed measurement calibration method can be successfully applied in the experiments with different scale and parameters.

5 Conclusion

A new calibration method is presented that provides validation of full-field, stereo DIC measurement systems in an industrial environment in a way that is traceable to the length standard. It is hoped that adoption of this method will increase the acceptance of DIC as a measurement method alongside other recognized traceable measurements, such as electrical resistance strain gauges and physical artifacts. The work performed demonstrates that displaying the speckle pattern on screen does not introduce large additional errors. Although the accuracy of the method is heavily dependent on the uncertainty of pixel pitch measurements and the construction of the screen used to display the speckle pattern, off-the-shelf technology can be used readily with sufficient accuracy to quickly and easily validate displacements *in situ*.

Acknowledgments

The authors wish to acknowledge the Metrology Workgroup of the French CNRS research network 2519 “Mesures de champs et identification en mécanique des solides/Full-field measurements and identification in solid mechanics” for use of the artificially generated reference speckle image used in this work.

References

1. M. Helfrick et al., “3D digital image correlation methods for full-field vibration measurement,” *Mech. Syst. Signal Process.* **25**(3), 917–927 (2011).
2. W. Wang et al., “Finite element model updating from full-field vibration measurement using digital image correlation,” *J. Sound Vib.* **330**(8), 1599–1620 (2011).
3. E. Patterson et al., “Calibration and evaluation of optical systems for full-field strain measurement,” *Opt. Lasers Eng.* **45**, 550–564 (2007).
4. SPOTS, “Guidelines for the calibration and evaluation of optical systems for strain measurement,” www.opticalstrain.org (2010).
5. E. Patterson et al., “A challenge for high-performance full-field strain measurement systems,” *Strain* **43**, 167–180 (2007).
6. C. Sebastian and E. Patterson, *Calibration of a Digital Image Correlation System Experimental Techniques*, John Wiley & Sons, Ltd., Hoboken, New Jersey (2012).
7. VANESSA Project, “CEN workshop agreement CEN/WS 71 validation of computational solid mechanics models,” 2014, <http://www.engineeringvalidation.org/?download=CWA%20VANESSA.pdf> (June 2014).
8. Y. Su et al., “Fourier-based interpolation bias prediction in digital image correlation,” *Opt. Express* **23**, 19242–19260 (2015).
9. E. Szigeti, “Improvements in or relating to digital image correlation systems,” Airbus Operations Limited, assignee, Patent EP3026632A2 (2016).
10. Apple Inc., “Apple iPad air tech specs,” 2014, from Apple UK, <https://www.apple.com/uk/ipad-air/specs/> (2014).
11. Amazon.co.uk, Inc., “Kindle paperwhite, 6” high resolution display (212 ppi) with built-in light, Wi-Fi (previous generation-6th),” 2016, from Amazon.co.uk, <https://www.amazon.com/Paperwhite-Resolution-Display-Previous-Generation/dp/B00JG8GBDM> (2016).
12. C. R. Nave, “Thermal expansion coefficients at 20 C,” 2014, from HyperPhysics (C.R. Nave, 2012), <http://hyperphysics.phy-astr.gsu.edu/hbase/tables/thexp.html> (2012).
13. M. A. Sutton, J. J. Orteu, and H. W. Schreier, *Image Correlation for Shape, Motion and Deformation Measurements: Basic Concepts, Theory and Applications*, Chapter 3–4, Springer Science+Business Media, LLC, New York (2009).
14. GDR CNRS 2519 Workgroup ‘Metrology,’ “Image data-base: strain2013,” 2014, from GDR CNRS 2519 Mesures de Champs et Identification en Mécanique des Solides, http://www.gdr2519.cnrs.fr/image_database/Strain2013/ (2013).
15. P. Reu, “A method for overlapping two DIC views by using a two-tone speckle pattern,” in *Advancement of Optical Methods in Experimental Mechanics*, Vol. 3, pp. 119–124, Springer International publishing AG, Cham, Switzerland (2014).
16. H. W. Schreier, J. Braasch, and M. A. Sutton, “Systematic errors in digital image correlation caused by intensity interpolation,” *Opt. Eng.* **39**, 2915–2921 (2000).
17. AG Neovo, “AG Neovo RX-W32 product datasheet,” 2014, from AG Neovo, http://global.agneovo.com/pdf/datasheet/RX-W32_DS_RXW3B0_V050_20120101.pdf (2012).
18. LG Inc., “42 LG ULTRA HD 4K TV Tech Specs,” 2016, from LG UK, <http://www.lg.com/uk/tvs/lg-42UB820V> (2016).

Biographies for the authors are not available.